Detection of solar wind-produced water in irradiated rims on silicate minerals

John P. Bradley[a,b,1], Hope A. Ishii[a,b], Jeffrey J. Gillis-Davis[b], James Ciston[c], Michael H. Nielsen[d,e], Hans A. Bechtel[f], and Michael C. Martin[f]

[a]Institute of Geophysics and Planetary Physics, Lawrence Livermore National Laboratory, Livermore, CA 94550; [b]Hawaii Institute of Geophysics and Planetology, University of Hawaii at Manoa, Honolulu, HI 96822; [c]National Center for Electron Microscopy, [d]Materials Science Division, and [f]Advanced Light Source Division, Lawrence Berkeley National Laboratory, Berkeley, CA 94720; and [e]Department of Materials Science and Engineering, University of California, Berkeley, CA 94720

Edited by Mark H. Thiemens, University of California at San Diego, La Jolla, CA, and approved December 23, 2013 (received for review October 25, 2013)

The solar wind (SW), composed of predominantly ~1-keV H^+ ions, produces amorphous rims up to ~150 nm thick on the surfaces of minerals exposed in space. Silicates with amorphous rims are observed on interplanetary dust particles and on lunar and asteroid soil regolith grains. Implanted H^+ may react with oxygen in the minerals to form trace amounts of hydroxyl (−OH) and/or water (H_2O). Previous studies have detected hydroxyl in lunar soils, but its chemical state, physical location in the soils, and source(s) are debated. If −OH or H_2O is generated in rims on silicate grains, there are important implications for the origins of water in the solar system and other astrophysical environments. By exploiting the high spatial resolution of transmission electron microscopy and valence electron energy-loss spectroscopy, we detect water sealed in vesicles within amorphous rims produced by SW irradiation of silicate mineral grains on the exterior surfaces of interplanetary dust particles. Our findings establish that water is a byproduct of SW space weathering. We conclude, on the basis of the pervasiveness of the SW and silicate materials, that the production of radiolytic SW water on airless bodies is a ubiquitous process throughout the solar system.

solar wind radiolysis | prebiotic water | cosmic dust | astrobiology | aberration-corrected scanning transmission electron microscopy

There are two principal space weathering processes, solar wind (SW) ion irradiation and micrometeorite impacts, that produce rims on exposed mineral surfaces (1). Our focus here is on SW irradiation because of its possible connection to the production of water and hydroxyl radicals (2–5). Space-weathered rim thicknesses vary with the densities of implanted solar flare (SF) tracks, and track densities depend on the exposure ages of individual interplanetary dust particles (IDPs) in space. On lunar soil grains and grains on surfaces of IDPs, rims are typically 75–150 nm thick with SF track densities of 10^{10}–10^{11} cm^{-2} that are consistent with 10^4- to 10^5-y SW exposure ages (6, 7) (Fig. 1 *B–D*). Rims on asteroid Itokawa regolith grains are 30–60 nm thick with SF track densities of 5×10^9 cm^{-2} that are consistent with ~10^3-y exposure ages (8) (*Origins and Properties of Rims on IDPs, Asteroid Itokawa, and Lunar Soil Grains*). This correlation between amorphous rim thicknesses and SF track densities indicates that SW irradiation is the primary mechanism for amorphous rim formation. We examine rims on surface grains in IDPs because they are solely due to SW irradiation, whereas rims on lunar soil grains are due to SW irradiation, impact vapor deposition, or a combination of both (9), and remote observations suggest that if water is indeed produced in rims on lunar soil grains, it is not efficiently retained (10). Typical 5- to 25-μm diameter chondritic porous (CP) IDPs are low-density aggregates of predominantly submicrometer-sized grains, and they are collected in the stratosphere (11) (Fig. 1 *A–D* and *Origins of CP IDPs*). Chemical analyses of the rims on silicate grains at the surfaces of IDPs reveal that SW sputtering breaks atomic bonds and selectively removes cations (e.g., Mg), leaving a stoichiometric excess of oxygen and rendering the rims chemically reactive. Similar cation depletions and oxygen excesses are observed in amorphous rims produced during laboratory irradiation of crystalline silicate standards using H^+ and He^+ ions at SW fluences (12).*

Previous attempts to detect water in rims on the surfaces of irradiated oxygen-rich minerals using bulk analytical methods, where water, if present, is close to detection limits, have yielded conflicting results (13, 14). We used valence electron energy-loss spectroscopy (VEELS) because its ability to detect water in situ at the nanoscale has been demonstrated in aqueous liquids, biomaterials, and ices (15–17). VEELS characterizes the low-loss region of the energy loss spectrum (0–50 eV), where features due to plasmons, valence band transitions, −OH, and H_2O can be observed (12, 15–19). We detect water in the SW amorphous rims on nominally anhydrous CP IDPs. To confirm this identification and to evaluate the VEEL spectra water features as a function of local solid-state environment and incident electron dose, we compare our results from the IDPs with three sets of standards: man-made liquid cells, empty and water-filled (20); talc, a hydrous mineral [$Mg_3Si_4O_{10}(OH)_2$]; and H^+- and He^+-irradiated anhydrous silicates (a description of the liquid cell is provided in *Materials and Methods*).

Results

VEEL spectra from the empty and water-filled liquid cells and talc are compared in Fig. 2 *A–C*. The spectrum from the empty cell contains a single feature peaked at 23 eV, the volume plasmon,

Significance

Whether water is produced by solar wind (SW) radiolysis has been debated for more than four decades. In this paper, we exploit the high spatial resolution of electron microscopy and sensitivity of valence electron energy-loss spectroscopy to detect water (liquid or vapor) in vesicles within (SW-produced) space-weathered rims on interplanetary dust particle (IDP) surfaces. Water in the rims has implications for the origin of water on airless bodies like the Moon and asteroids, the delivery of water to the surfaces of terrestrial planets, and the production of water in other astrophysical environments. In particular, water and organic carbon were likely delivered simultaneously by the high flux of IDPs accreted by the early Earth and other terrestrial planets.

Author contributions: J.P.B., M.H.N., H.A.B., and M.C.M. performed research; H.A.I., J.J.G.-D., J.C., H.A.B., and M.C.M. analyzed data; and J.P.B., H.A.I., J.J.G.-D., J.C., and M.H.N. wrote the paper.

The authors declare no conflict of interest.

This article is a PNAS Direct Submission.

[1]To whom correspondence should be addressed. E-mail: johnbrad@hawaii.edu.

This article contains supporting information online at www.pnas.org/lookup/suppl/doi:10.1073/pnas.1320115111/-/DCSupplemental.

*Topanni A, Dukes C, Baragiola R, Bradley JP (2006) 37th Lunar Planet Sci Conf, March 13–17, 2006, League City, TX, abstr. 2056.

Downloaded by guest on October 16, 2021

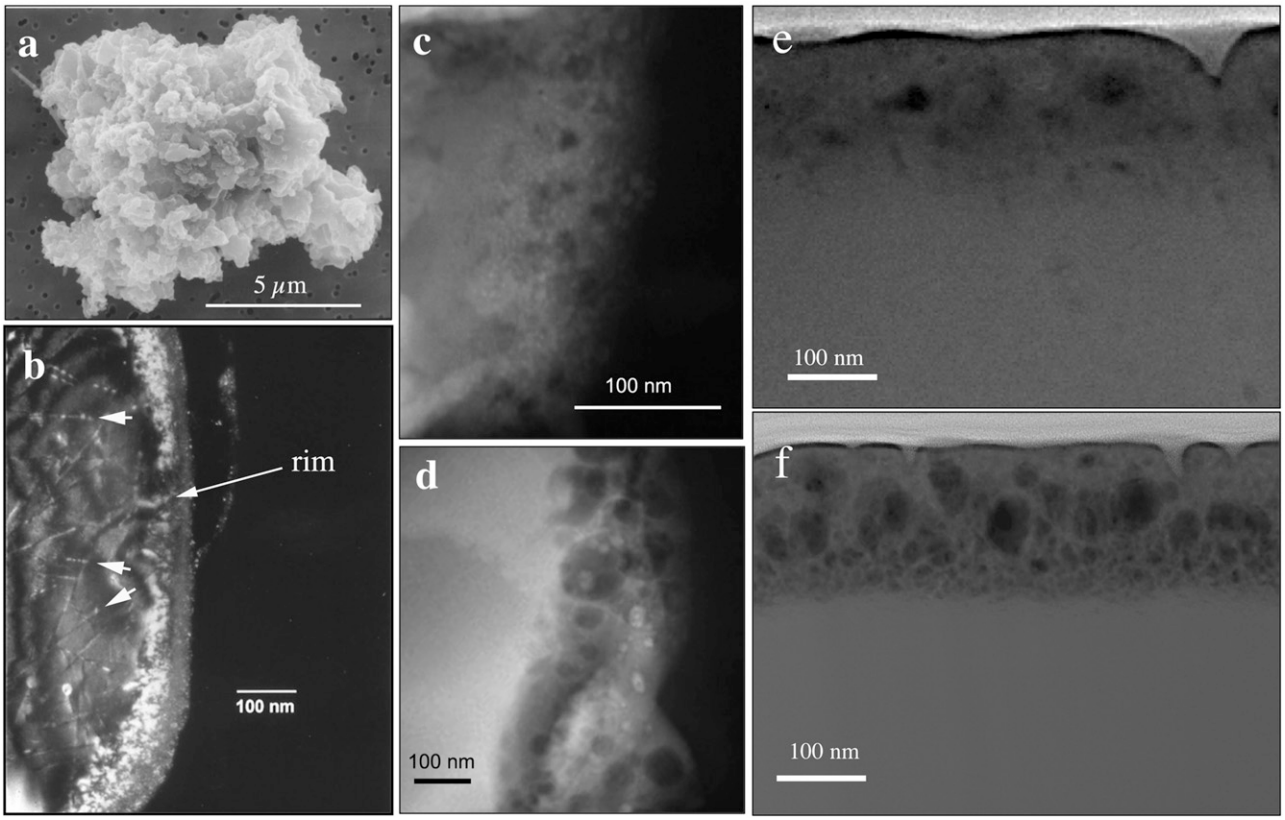

Fig. 1. (*A*) Secondary electron image of CP IDP U220A19. (*B*) Dark-field image of a pyroxene crystal on the surface of U220A19 with an ~100-nm thick amorphous rim resulting from SW irradiation. The linear features (arrows) in the pyroxene crystal are SF tracks. (*C*) High-angle annular dark-field (HAADF) density contrast image of the SW rim on the pyroxene showing vesicles within the amorphous silicate rim. (*D*) HAADF image of a vesiculated rim on a lunar soil anorthite crystal. Water was not detected in the vesicles. HAADF images of the amorphous rims on the surfaces of olivine (*E*) and anorthite (*F*) crystals following exposure to 5-keV He^+ (7.5×10^{18} He^+ per square centimeter) and 5-keV H^+ (1.0×10^{19} H^+ per square centimeter), respectively.

that is directly related to the specimen dielectric function (18). With water in the cell, a feature appears at 8.5 eV, and a second feature at 13.5 eV with fine structure extending to ~16 eV is sometimes observed. Depending on specimen thickness, a much weaker and broader third feature at 4.3 eV is observed. The 4.3-eV feature corresponds to the ionization threshold (IT) of water, the 8.5-eV feature corresponds to the energy gap (EG) of water, and the 13.5-eV feature is the hydrogen (H-K) core scattering edge (15–17, 21, 22).

Talc is thermally sensitive like other hydrated layer-lattice silicates that contain structurally bound water, and it decomposes in the electron beam to form enstatite ($MgSiO_3$), silica (SiO_2), and unbound water (H_2O) (23). Using VEELS, we monitored unbound water accumulation as a function of electron dose (Fig. 2 *D–F*). At low beam currents (0.05 nA), no water features are evident, but as the current is increased, both the IT and H-K edge features appear in conjunction with visible bubbling (rapid vesicle growth). A similar dependence of water features on electron dose and bubbling is observed when water ice is melted in the electron beam (16, 17).

The laboratory-irradiated anhydrous silicate mineral standards are olivine ($[Mg,Fe]_2SiO_4$), clinopyroxene ($[Ca,Mg,Fe]SiO_3$), and anorthite ($CaAl_2Si_2O_8$) (*Materials and Methods* and *SI Materials and Methods*). Both H^+- and He^+-irradiated standards have ~100-nm thick amorphous rims on their surfaces that contain vesicles 10–50 nm in diameter (Fig. 1 *E* and *F*). VEEL spectra from the rims differ from those from underlying mineral substrates (Fig. 2 *G–J*). The substrate spectra have relatively narrow volume plasmon peaks, typical of crystalline silicates, with weak surface plasmons between 8 eV and 12 eV originating from the upper and lower surfaces of the thin specimen. The volume plasmon peaks from the rims are significantly broader and are often shifted to a lower energy because surface plasmon contributions are greater due to irradiation-induced atomic-bond disruption, the presence of vesicles, and nanoporosity (12, 18, 19). Water IT, EG, and H-K features are observed in some vesicles in H^+-irradiated rims but not in He^+-irradiated rims, where, instead, the He-K core scattering edge at ~22 eV is observed in some vesicles (Fig. 2 *G–J*). A higher abundance of water-bearing vesicles was noted in the irradiated anorthite standard relative to the pyroxene and olivine standards.

VEEL spectra water features are similarly detected in amorphous rims and in vesicles contained within the rims on silicate grains in several CP IDPs (*Materials and Methods* and *SI Materials and Methods*). Fig. 3 *A–C* shows successive spectra from a vesicle at the base of the rim on a pyroxene crystal in CP IDP U220A19. Water IT, EG, and H-K features remain prominent until the electron beam perforates the vesicle, and they abruptly disappear as water escapes to vacuum. Spectra from the rim exhibit IT and EG features, and the pyroxene crystal exhibits only weak surface plasmons (Fig. 3 *D* and *E*). Relative to the spectrum from the pyroxene crystal, the rim spectra have a significantly broader plasmon peak shifted downward in energy by ~2 eV. A vesicle in the rim on another IDP (U2001 D7) exhibits IT, EG, and double-peaked H-K features, and the amorphous rim alongside the vesicle exhibits an IT feature (Fig. 3 *F* and *G*). We estimated the abundance of water in rims by X-ray energy dispersion spectroscopy (EDS) quantification of elemental abundances. Some SW rims on IDPs have up to 12 atomic percent excess O relative to oxide stoichiometry, attributable to, at most, ~1 weight percent water in the rims (*SI Materials and Methods*).

Downloaded by guest on October 16, 2021

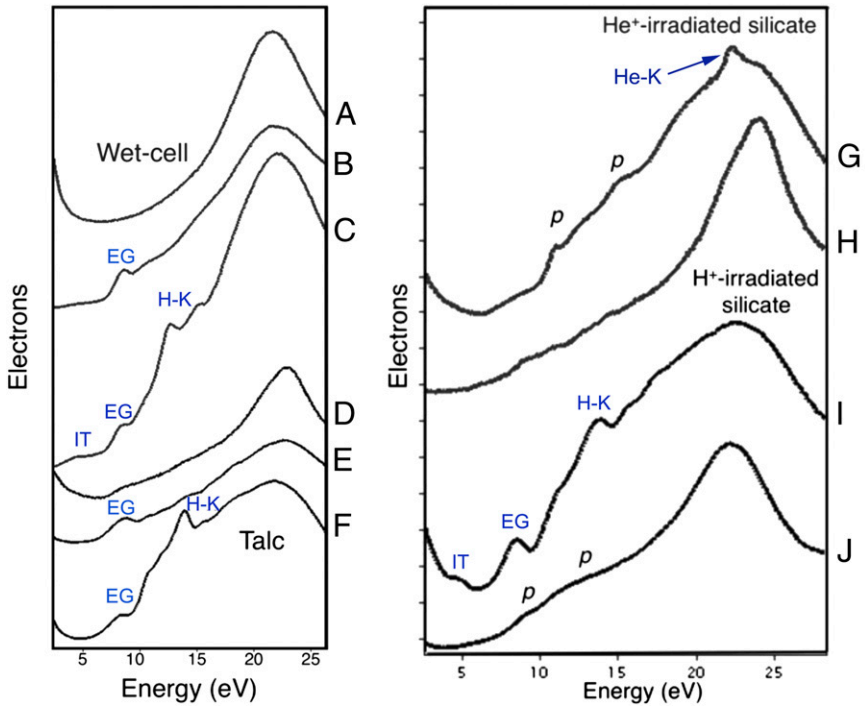

Fig. 2. VEEL spectra from an empty liquid cell (*A*) and two different locations in the water-filled cell (*B* and *C*). VEEL spectra from talc acquired over a constant time interval using a beam current of 0.05 nA (*D*), 0.15 nA (*E*), and 0.25 nA (*F*) are shown. (*G* and *H*) VEEL spectra from He^+-irradiated rim and olivine substrate. (*I* and *J*) Spectra from H^+-irradiated rim and anorthite substrate. IT, water IT; H-K, H-K core edge; *p*, surface plasmons. The beam current is ~0.05 nA for *G*–*I*. Details of mineral irradiation by He^+ and H^+ are provided in *SI Materials and Methods*.

Discussion

We find that detection of structurally unbound water in minerals using VEELS depends on the local physical environment of the water and incident electron dose. In a liquid cell, where water is not laterally confined, the position of the EG feature varies from 8 to 9 eV and the H-K feature may or may not be observed (15) (Fig. 2 *A*–*C*). With talc, the appearance of these features depends on electron dose and bubble formation, similar to water ice (Fig. 2 *D*–*F*). With water sealed in vesicles in SW rims, IT, EG, and H-K features are often immediately apparent even at low electron doses (e.g., Fig. 3 *A* and *B*). Prior studies of the VEEL spectra from liquid water and their degradation byproducts are sparse: Water dissociates in the electron beam, forming transient species that include H^+, $O^•$, $OH^•$, $H^•$, H_2, H_2O_2, and $HO_2^•$ (15–17). VEELS of molecular oxygen and hydrogen, which exhibit features at 13 eV and 15 eV, respectively, show that these peak positions are perturbed by formation of other stable molecules (e.g., CO, CO_2), which leads to an increase in the binding energy due to charge screening of the positive oxygen core (24). We attribute variations in the VEEL spectra water features to similar effects because, in addition to water, the rims and vesicles almost certainly contain Si-OH and possibly other species (e.g., carbon compounds) that were recoil-implanted into the rims by the SW.

Our detection of SW-produced water in rims on silicate mineral grains in nominally anhydrous IDPs has implications for production of water on the surfaces of airless bodies, its delivery to the surface of the Earth and other terrestrial planets, and production of water in the interstellar medium (3–5, 13).[†] For example, there is intense interest in water at the poles of the Moon (10, 25–27). A fundamental and as-yet unresolved question is the source of the water. Three sources have been proposed (*i*) primordial water present when the Moon formed and now sequestered in the lunar regolith, (*ii*) impacts by ice-rich comets and wet asteroids, and (*iii*) in situ water formation on the surfaces of oxygen-rich lunar mineral grains exposed to SW H^+ (1–3, 10, 25, 26). The sample analyses presented here, together with remotely sensed observations (10, 26), yield supporting evidence for the in situ creation of OH/H_2O by SW radiolysis of the lunar regolith. Previous sample studies have described the mechanism by which the SW could produce hydroxyl in the lunar regolith (5, 25). This study establishes that the SW does produce water in rims on silicate minerals. Although the VEELS data presented here are from CP IDPs, silicates and SW are common to both the Moon and asteroids. Hence, we infer that a similar process of creation of water must be occurring on these airless bodies, consistent with both our experimental findings and the lunar remote-sensing data. For example, anorthite is the most oxygen-rich of the silicates we examined, and we observed the highest abundance of vesicles with detectable water in the H^+-irradiated rim on the anorthite standard. The Moon-mineralogy imaging spectrometer detected the strongest hydroxyl absorption features associated with fresh craters in the anorthite-rich lunar highlands (26).

Although the remote observational data and our IDP sample analysis provide compelling evidence that the SW produces lunar water, detecting it in rims on lunar grains is expected to be challenging. Apart from at least two processes implicated in lunar rim formation (9), remote spectral data from the National Aeronautics and Space Administration's EPOXI mission (10) reveal a dynamic diurnal process of hydration, dehydration, and rehydration of the lunar regolith as a function of surface temperature that exceeds 100 °C in midlatitude regions. Typical CP IDPs, on the other hand, are from small frozen (cometary) parent bodies, and they can remain cold (≤10 °C) during their 10^4- to 10^5-y exposures to the SW while in solar orbit. They are pulse-heated for several seconds during entry, but the survival of

[†]Daulton TL, Bernatowicz TJ, Croat TK (2012) 43rd Lunar Planet Sci Conf, March 19–23, 2012, The Woodlands, TX, abstr. 2247.

EARTH, ATMOSPHERIC, AND PLANETARY SCIENCES
Downloaded by guest on October 16, 2021

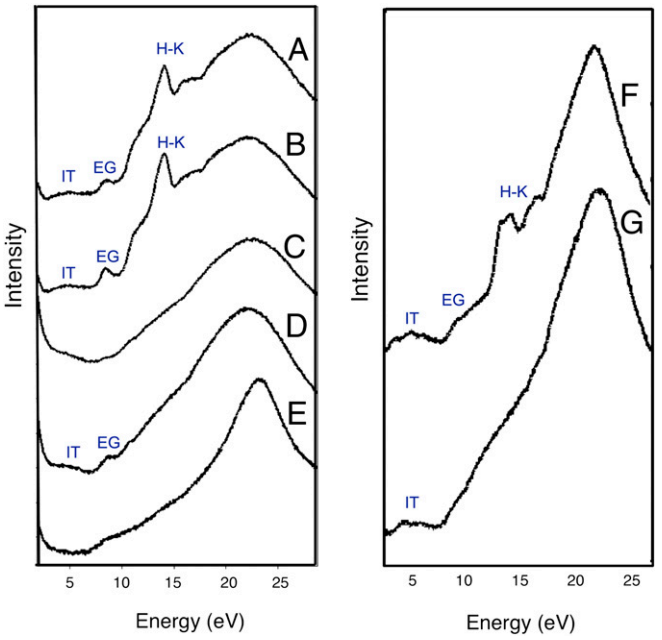

Fig. 3. VEEL spectra from an SW rim on a pyroxene ($Mg_{0.7}Fe_{0.3}SiO_3$) in CP IDP U220A19 using a defocused and monochromated beam with a 0.05-nA current. (*A* and *B*) Spectra obtained sequentially from a vesicle in the rim. (*C*) Spectrum from the vesicle following perforation by the electron beam. (*D*) Spectrum from the amorphous silicate rim on the pyroxene. (*E*) Spectrum from the underlying pyroxene crystal substrate. (*F*) Spectra from a vesicle in a rim on a pyroxene crystal. (*G*) Amorphous rim alongside the vesicle in CP IDP U2001 D7. Beam currents used were 0.05–0.1 nA.

SF tracks, near-saturation levels of implanted solar noble gases (He, Ne, and Ar), and volatile organic compounds show that low-density, highly porous CP IDPs can enter the atmosphere with minimal heating (11, 28–30) (Fig. 1*B*).

Water in rims on the surfaces of IDPs has implications for the delivery of water to the surfaces of terrestrial planets. The CP subset of IDPs studied here is part of the population of micrometeorites from comets and asteroids that continuously enter the Earth's atmosphere (*Origins of CP IDPs*). The present-day flux (30,000–40,000 tons/y) is comparable to, and possibly greater than, that of centimeter-to-kilometer size meteoritic objects from asteroids and comets; the flux may have been much higher on the early Earth (30, 31). Thus, some CP IDPs contribute both water and organic carbon simultaneously to the surface of the Earth and the other terrestrial planets.

Materials and Methods

We examined amorphous rims on the surfaces of H^+- and He^+-irradiated anhydrous silicate mineral standards and compared them with amorphous rims on anhydrous CP IDPs using an 80- to 300-keV aberration-corrected scanning transmission electron microscope equipped with a monochromator and high-resolution electron energy-loss spectrometer (*SI Materials and Methods*). IDPs were prepared by thin sectioning using ultramicrotomy (7) and by direct dispersion of disaggregated grains onto thin carbon films. The surfaces of polished thick-flat specimens of the mineral standards were irradiated using 5-keV H^+ and He^+ ions at fluences duplicating typical SW exposure ages (*SI Materials and Methods*). Electron-transparent cross-sections were harvested from the irradiated silicates and an unirradiated hydrated silicate standard, talc, using a focused ion beam instrument. The talc standard was decomposed in the electron beam to generate water as a first water standard. A second water standard was prepared using a wet cell that consists of a pair of electron-transparent silicon nitride windows, each ~100 nm thick, with a thin film of water sealed between them (20). The microstructures of the rims were examined using bright-field and dark-field imaging, and their elemental compositions were measured using EDS (*SI Materials and Methods*).

ACKNOWLEDGMENTS. This work was funded by the National Aeronautics and Space Administration's Cosmochemistry and Laboratory Analysis of Returned Samples (LARS) programs. Portions of this work were performed at Lawrence Livermore National Laboratory under the auspices of the US Department of Energy under Contract DE-AC52-07NA27344 and at the National Center for Electron Microscopy and Advanced Light Source Division, which are supported by the Office of Science, Office of Basic Energy Sciences of the US Department of Energy under Contract DE-AC02-05CH11231.

1. Hapke B (2001) Space weathering from Mercury to the asteroid belt. *J Geophys Res* 106(E5):10039–10073.
2. Liu YY, et al. (2012) Direct measurement of hydroxyl in the lunar regolith and the origin of lunar surface water. *Nat Geosci* 5:779–782.
3. Ichimura AS, Zent AP, Quinn RC, Sanchez MR, Taylor LA (2012) Hydroxyl (OH) production on airless planetary bodies: Evidence from H^+/D^+ ion-beam experiments. *Earth Planet Sci Lett* 345:90–94.
4. Greenwood JP, et al. (2011) Hydrogen isotope ratios in lunar rocks indicate delivery of cometary water to the Moon. *Nat Geosci* 4:79–82.
5. Lucey P, et al. (2006) Understanding the lunar surface and space-moon interactions. *Reviews in Mineralogy and Geochemistry* 60(1):83–219.
6. Bradley JP, Brownlee DE, Fraundorf P (1984) Discovery of nuclear tracks in interplanetary dust. *Science* 226(4681):1432–1434.
7. Bradley JP, Brownlee DE (1986) Cometary particles: Thin sectioning and electron beam analysis. *Science* 231(4745):1542–1544.
8. Noguchi T, et al. (2011) Incipient space weathering observed on the surface of Itokawa dust particles. *Science* 333(6046):1121–1125.
9. Noble S, Keller LP, Peiters CM (2005) Evidence of space weathering in regolith breccias I: Lunar regolith breccias. *Meteorit Planet Sci* 40(3):397–408.
10. Sunshine JM, et al. (2009) Temporal and spatial variability of lunar hydration as observed by the Deep Impact spacecraft. *Science* 326(5952):565–568.
11. Bradley JP (2013) Early solar nebula grains—Interplanetary dust particles. *Meteorites and Cosmochemical Processes,* Treatise on Geochemistry, ed Holland HD, Turekian KK (Elsevier–Pergamon, Oxford), 2nd Ed, Vol 1, pp 287–308.
12. Bradley JP, Dai ZR (2009) An analytical SuperSTEM for extraterrestrial materials research. *Meteorit Planet Sci* 44(10):1627–1642.
13. Djouadi Z, et al. (2011) Hydroxyl radical production and storage in analogues of amorphous interstellar silicates: A possible "wet" accretion phase for inner telluric planets. *Astron Astrophys* 531:A96–A104.
14. Burke DJ, et al. (2011) Solar wind contribution to surficial lunar water: Laboratory investigations. *Icarus* 211(2):1082–1088.
15. Jungjohann KL, Evans JE, Aguiar JA, Arslan I, Browning ND (2012) Atomic-scale imaging and spectroscopy for in situ liquid scanning transmission electron microscopy. *Microsc Microanal* 18(3):621–627.
16. Leapman RD, Sun S (1995) Cryo-electron energy loss spectroscopy: Observations on vitrified hydrated specimens and radiation damage. *Ultramicroscopy* 59(1-4):71–79.
17. Aronova MA, Sousa AA, Leapman RD (2011) EELS characterization of radiolytic products in frozen samples. *Micron* 42(3):252–256.
18. Yin NYS, Wang ZL (1999) Plasmon energy shift in mesoporous and double length-scale ordered nanoporous silica. *Appl Phys Lett* 74(18):2629–2631.
19. Hojou TK, Furuno S, Kuchita KN, Sasajima N, Izui K (1998) EELS analysis of SiC crystals under hydrogen and helium dual-ion beam irradiation. *Nucl Instrum Methods Phys Res B* 141(1-4):148–153.
20. Nielsen MH, et al. (2012) Structural evolution, formation pathways and energetic controls during template-directed nucleation of $CaCO_3$. *Faraday Discuss* 159:105–121.
21. Grand D, Bernas A, Amouyal E (1979) Photoionization of aqueous indole: Conduction band edge and energy gap in liquid water. *Chem Phys* 44(1):73–79.
22. Farhataziz H, Rodgers MAJ, eds (1987) *Radiation Chemistry—Principles and Applications* (VCH, New York).
23. De Souza H, Yada K (1988) Thermal transformation of talc as studied by electron-optical methods. *Clays Clay Miner* 36:289–297.
24. Crozier PA, Chenna S (2011) In situ analysis of gas composition by electron energy-loss spectroscopy for environmental transmission electron microscopy. *Ultramicroscopy* 111(3):177–185.
25. Hibbitts CB, et al. (2011) Thermal stability of water and hydroxyl on the surface of the Moon from temperature-programmed desorption measurements of lunar analog materials. *Icarus* 213(1):64–72.
26. Pieters CM, et al. (2009) Character and spatial distribution of OH/H2O on the surface of the Moon seen by M3 on Chandrayaan-1. *Science* 326(5952):568–572.
27. Greenwood JP, et al. (2011) Hydrogen isotope ratios in lunar rocks indicate delivery of cometary water to the Moon. *Nat Geosci* 4:79–82.
28. Brownlee DE (1985) Cosmic dust—Collection and research. *Annual Review of Earth and Planetary Sciences* 13:147–173.
29. Matrajt G, Messenger S, Brownlee DE, Joswaik DJ (2012) Diverse forms of primordial organic matter identified in interplanetary dust particles. *Meteorit Planet Sci* 47(4):529–549.
30. Love SG, Brownlee DE (1993) A direct measurement of the terrestrial mass accretion rate of cosmic dust. *Science* 262(5133):550–553.
31. Nesvorny D, et al. (2010) Cometary origin of the zodiacal cloud and carbonaceous micrometeorites. Implications for hot debris disks. *Astrophys J* 713(2):816–836.

Downloaded by guest on October 16, 2021